

Formation and Evolution of a Freshwater Plume in the Northwestern Tropical Atlantic in February 2020

G. Reverdin¹ , L. Olivier¹ , G. R. Foltz², S. Speich³ , J. Karstensen⁴ , J. Horstmann⁵, D. Zhang⁶ , R. Laxenaire⁷ , X. Carton⁸, H. Branger⁹ , R. Carrasco⁵ , and J. Boutin¹ 

¹LOCEAN-IPSL, Sorbonne Université-CNRS-IRD-MNHN, Paris, France, ²NOAA/Atlantic Oceanographic and Meteorological Laboratory, Miami, FL, USA, ³Laboratoire de Météorologie Dynamique, ENS-Ecole Polytechnique-CNRS-Sorbonne Université, Paris, France, ⁴GEOMAR Helmholtz Centre for Ocean Research Kiel, Kiel, Germany, ⁵Helmholtz-Zentrum Geesthacht, Geesthacht, Germany, ⁶CICOES/University of Washington and NOAA/Pacific Marine Environmental Laboratory, Seattle, WA, USA, ⁷Center for Ocean-Atmospheric Prediction Studies, Florida State University, Tallahassee, FL, USA, ⁸Laboratoire d'Océanographie Physique et Spatiale, UBO-CNRS-IFREMER-IRD, Plouzané, France, ⁹IRPHE, CNRS-AMU, Luminy, France

Key Points:

- First direct observation of a freshwater plume separating from the shelf near Demerara Rise in early February
- The 2020 plume carried 0.15 Sv of freshwater northward during 10 days and after 14 days, covered more than 100,000 km²
- Plume probably initiated by wind direction shift closer to the equator, 5–7 days earlier and stirred by a North Brazil Current ring

Supporting Information:

Supporting Information may be found in the online version of this article.

Correspondence to:

G. Reverdin,
gilles.reverdin@locean.ipsl.fr

Citation:

Reverdin, G., Olivier, L., Foltz, G. R., Speich, S., Karstensen, J., Horstmann, J., et al. (2021). Formation and evolution of a freshwater plume in the northwestern tropical Atlantic in February 2020. *Journal of Geophysical Research: Oceans*, 126, e2020JC016981. <https://doi.org/10.1029/2020JC016981>

Received 14 NOV 2020
 Accepted 17 MAR 2021

Abstract In February 2020, a 120-km-wide freshwater plume was documented by satellite and in situ observations near the Demerara Rise (7°N/54°W–56°W). It was initially stratified in the upper 10 m with a freshwater content of 2–3 m of Amazon water distributed down to 40 m. On February 2nd, ship transects indicate an inhomogeneous shelf structure with a propagating front in its midst, whereas minimum salinity close to 30 pss was observed close to the shelf break on February 5th. The salinity minimum eroded in time but was still observed 13–16 days later with 33.3 pss minimum value up to 400 km from the shelf break. At this time, the mixed layer depth was close to 20 m. The off-shelf flow lasted 10 days, contributing to a plume area extending over 100,000 km² and associated with a 0.15 Sv (10⁶ m³ s⁻¹) freshwater transport. The off-shelf plume was steered northward by a North Brazil Current ring up to 12°N and then extended westward toward the Caribbean Sea. Its occurrence followed 3 days of favorable wind direction closer to the Amazon estuary, which contributed to north-westward freshwater transport on the shelf. Other such events of freshwater transport in January–March are documented since 2010 in salinity satellite products in 7 out of 10 years, and in 6 of those years, they were preceded by a change in wind direction between the Amazon estuary and the Guianas favoring the north-westward freshwater transport toward the shelf break.

Plain Language Summary This study documents how freshwater from the Amazon reaches the deep ocean up to 12°N in the northwest tropical Atlantic in January–March. The classical view is that the water is channeled along the shelf to the Caribbean Sea. Here, we document a freshwater plume from in situ and satellite observations during the EUREC4A-OA/ATOMIC program in 2020. This plume separated from the shelf near 55°W north of French Guiana on February 2–5. This fresher water was stirred by a North Brazil Current ring up to 12°N before mostly spreading westward. The near-surface water was initially very stratified at least until 10-m from the surface. More than 14 days later and 400 km farther north, salinity as low as 33.3 pss with mixing depths on the order of only 20-m was still encountered. The total area of the freshwater plume reached 100,000 km² with a flow of freshwater on the order of 0.15 Sv (10⁶ m³ s⁻¹) during 10 days. This phenomenon seems to be triggered by changes in the wind direction on the shelf closer to the equator, and has also been observed in satellite products in 7 out of 10 years since 2010.

1. Introduction

The main topic of this study is the freshwater transport from the Guiana shelves to the Northwest Tropical Atlantic in boreal winter and the processes that control this transport. Fresher surface layers are often relatively thin and induce strong stratification in the upper ocean layers, limiting the turbulent heat and momentum fluxes across the base of the mixed layer. In winter, this condition has the potential to enhance near-surface cooling by sensible and latent surface heat fluxes and the trapping of momentum enabling the development of barrier layers and temperature inversions at the base of the halocline (Mignot et al., 2012). Freshwater originating from the shelves also carries nutrients and organic matter that sustain food webs.

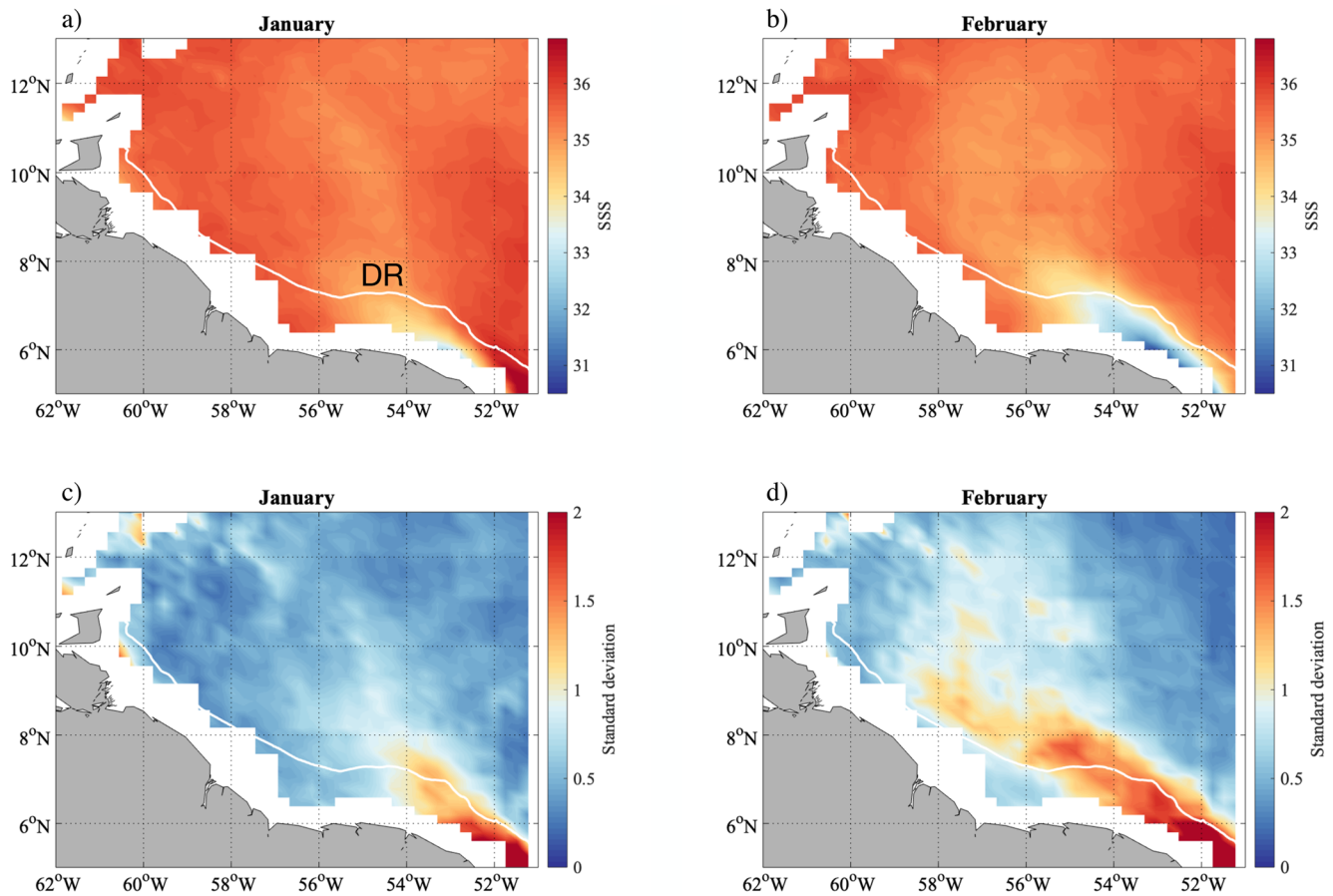


Figure 1. Average salinity and its standard deviation based on weekly satellite sea surface salinity (Climate Change Initiative products) in 2010–2019. Upper panels: averages for January and February, and lower panels the corresponding standard deviations. DR indicates Demerara Rise location.

The freshwater input by the Amazon and other northeastern South American rivers is minimal in December and progressively increases from January to May. During this period, the North Brazil Current (NBC) retroflexion is either non-existent or weak. As a consequence, January through March is the season of maximum salinity in the northwestern tropical Atlantic west of 45°W, with no offshore transport of freshwater at the NBC retroflexion, and with salty water flowing along the continental slope of the Guiana shelves. This is also the season of minimal plume extension (defined by salinity less than 35.5 ps) according to Fournier et al. (2017). However, even in this season, occasional freshwater transport from the shelves, either induced by eddies or the winds (via the Ekman transport), might lead to the development of surface freshened layers, although the associated barrier layers are mostly found north of 10°N (Mignot et al., 2012).

Pathways of freshwater transport have also been documented using data from surface drifters (Muller-Karguer et al., 1988) and profiling floats (Hu et al., 2004), which illustrate large seasonal variability of the pathways. It is usually expected that in the early part of the year, the freshwater pathway along the Guiana shelves and into the Caribbean Sea is favored. This is also documented in the model and data study of Coles et al. (2013) with freshwater mostly trapped on the shelf and no clear evidence from historical CTDs of fresh surface layers offshore of the shelves.

Satellite surface imagery (L-band radiometry) illustrates that this off-shore freshwater transport does not happen frequently in January (Figures 1a and 1b), but that it is often present in February (Figures 1c and 1d) and later in the year. In February, the weekly sea surface salinity (SSS) product used here for 2010–2019 shows a band of maximum variability near the shelf break between 54°W and 58°W and peaking near 55°W. Though the maximum is within 100 km of the shelf break, the increase in variability compared to January

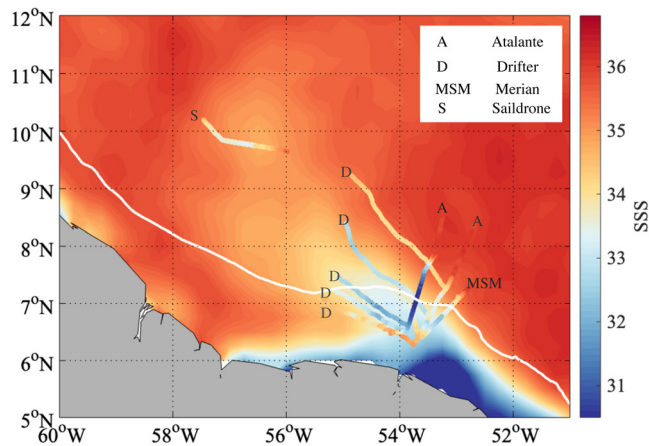


Figure 2. Average for February 2–19, 2020 of the daily salinity fields based on SMOS and SMAP satellite data, overlaid with the data collected by the various observing platforms within the fresh plume (A for R/V Atalante on February 2 and 5, Maria S. Merian (MSM) for R/V MSM on February 2; D for drifters on February 2–7 and S for Sairdron during February 16–18). The different tracks/trajectories are color-coded with observed surface salinity.

extends all the way to 12°N in the longitude range 54.5°W–58°W, and it is associated with intermittent fresh plumes. This contributes to lowering the average surface salinity in this offshore region.

Pathways of surface freshened layers originating from the shelves and ultimately from the Amazon have been followed in the past using satellite ocean color imagery (Hu et al., 2004; Müller-Karger et al., 1988) and more recently the L-band microwave imagery of surface salinity (Fournier et al., 2015, 2017; Grodsky et al., 2014; Salisbury et al., 2011). The study of Fratantoni and Glickson (2002) illustrates the entrainment of shelf water rich in Chla in the ocean interior around large intense anticyclonic eddies detached from the NBC in February 1999. These eddies were also investigated for hydrography by Johns et al. (2003).

These different studies highlight the importance of eddies in shaping where the transport of fresh shelf water to the deep ocean happens, in particular the role of anticyclonic eddies shed from the NBC retroflection near 8°N close to the Demerara Rise (DR), early in the year. These studies have also pointed out the sensitivity of the freshwater transport to wind magnitude and direction. Winds parallel to the coast and the shelf-break were found to be more favorable for offshore transport than wind perpendicular to the shore. Thus, during the early months of the year, when the atmospheric Inter-tropical Convergence Zone shifts southward, the dominant northeasterly winds are not favorable for this off-shelf transport east of 53°W.

However, quantifying advection and transport of surface freshwater in such analyses is hindered in two ways. First, color imagery is not a direct estimate of salinity (although Salisbury et al. [2011] and Fournier et al. [2015] show how this can be used). Second, the time averaging of the satellite products, in particular from L-Band, is often over one week or more, which is rather long to display the detailed processes involved in the freshwater transport. In this study, we explore the transport of fresh shelf water to the north in this region using novel in situ observations and high frequency satellite products. In early February 2020, during the Elucidating the Role of Clouds-Circulation Coupling in Climate Ocean-Atmosphere (EUREC⁴A-OA) experiment (Stevens et al., 2021), the RV Atalante and the RV Maria S. Merian (MSM) surveyed an area close to the Guiana shelf just as a plume of freshwater was ejected from the shelf to the deep ocean (Figure 2). The period investigated in this study spans from the 2nd to the 21st of February 2020, after which the surface freshened plume was less clear and there were less in situ or remote sensing data available.

2. Data

The data used include measurements collected by the two research vessels, by five instrumented drifters deployed into the freshwater plume, and by Uncrewed Surface Vehicle (USV) Sairdrones (Zhang et al., 2019) deployed for the EUREC⁴A-ATOMIC (Atlantic Tradewind Ocean Mesoscale Interaction Campaign) cruises and equipped to measure sea surface temperature (SST), SSS, and current profiles. The plume was also followed daily using satellite imagery (ocean color and salinity from L-band radiometry), as well as model simulations (Mercator PSY2V4) and satellite altimetry.

2.1. In Situ Data

Both RV Atalante and MSM continuously measured temperature (T) and salinity (S) from thermosalinographs pumping water near 5 m below the surface, and they measured wind with dedicated meteorological sensors. During crossings of the fresh plume on the 2nd and 4th–5th of February, either a moving vessel profiler (MVP) or a fast uCTD were deployed from RV Atalante and MSM, providing high resolution T and S vertical profile sections across the plume in the upper 50 m. The RV Atalante was also equipped with a 150 kHz RDI Acoustic Doppler current profiler (ADCP), providing currents 29 m below the sea surface. The MSM 75 kHz ADCP provided calibrated currents starting at 18.5 m below the sea surface (8-m bins).

A coherent-on-receive marine radar (MR) developed at the Helmholtz-Zentrum Geesthacht (Carrasco et al., 2017) was operated on board MSM for monitoring the surface roughness as well as the ocean surface currents in the vicinity of the vessel. The MR operates at X-band (9.4 GHz) with a pulse repetition of 2 kHz with vertical polarization. The pulse length of 50 ns results in a range resolution of 7.5 m and the 7.5' antenna array allows an azimuthal resolution of 0.9°. The radar was operated with an antenna rotation frequency of ~0.45 Hz covering a range distance of 3.2 km around the vessel, thus a 6.4 km width along the track of the vessel. The normalized backscatter intensity results from the temporal mean radar backscatter intensity at every point, which is normalized and corrected for range and wind direction dependencies (Dankert & Horstmann, 2007). As the normalized backscatter intensity is strongly dependent on the ocean surface roughness it depicts all structures that affect the surface roughness. In addition, the MR image sequences are utilized to retrieve the near-surface current (in approximately the upper 5 m) maps by analyzing the wave signal (Huang et al., 2016; Lund et al., 2018; Senet et al., 2001). Therefore, the MR image sequences are converted from the spatiotemporal domain to the wavenumber-frequency domain via a 3-D FFT. Within the wavenumber-frequency domain, the wave signal is located on the so-called dispersion shell. In the presence of a current, the Doppler effect leads to a translation and dilation of the dispersion shell. The current is determined using a fit that minimizes the wave signal's distance from the dispersion shell.

Between the two crossings of the plume, the two vessels surveyed a salinity-stratified area on the shelf. During this survey, the free-drifting platform Ocarina (Bourras et al., 2019) was deployed for a little more than 12 h. This platform was equipped with a 1,200 kHz ADCP to measure current profiles at 0.5 m resolution between 0.29 and 17.29 m from the sea surface. These data are combined with temperature and salinity profiles collected from the RV Atalante MVP to estimate the gradient Richardson number (R_i) in this stratified near-surface layer at different times of the day.

The five surface Velocity Program (SVP) drifters deployed in the plume were instrumented by the company "Pacific Gyre" to measure temperature and salinity every 30 min at 20-cm, 5-m, and 10-m depths. They also measured surface barometric pressure as well as wind speed and direction 0.5 m above the surface, with regular GPS positioning. Positions were edited for some erroneous data and are less certain for one drifter closer to the coast. Temperature and salinity data retrievals were good at 20-cm depth, with some early loss of data occurring at 5-m and 10-m depth. This was not an issue during the first 10 days of deployment except for one drifter not used here just to the north of the plume. For this investigation, the comparison of the three depth records does not suggest significant salinity biases.

A fleet of four USV SAILDRONES operated in the eddy-rich area north of the Guianas (9°N-12°N) and crossed the freshwater plume during 17th to 18th February. We use the position, temperature, salinity, and wind reported every minute, as well as the ocean velocity profiles (300 kHz RDI ADCP) averaged every 5 min from one NOAA SAILDRONE. The velocity profiles from 6 m down to a maximum depth of 104 m are provided with a 2-m resolution.

2.2. Satellite Data

The satellite data used are daily products of chlorophyll, mapped surface current from near-real time (NRT) DUACS-NRT altimetry products, and daily analyses of surface salinity based on a blend of data from different L-band radiometry satellite missions.

Daily chlorophyll-a (Chla) concentration maps on a spatial grid of 0.02° are provided by CLS (<https://data-store.cls.fr/catalogues/chlorophyll-high-resolution-daily>). The maps are composites built from four satellite sensors, VIIRS (on Suomi-NPP and NOAA-20 US platforms) and OLCI (on Sentinel 3A and 3B Copernicus European platforms). The VIIRS L1A products are downloaded from the NASA Ocean Color Web, whereas the OLCI L1 products are downloaded from the EUMETSAT Copernicus On-line Data Access in NRT. As described in Stum et al. (2015), the Polymer software (Steinmetz et al., 2011) is used since 2014 to compute Chla from the top of atmosphere reflectances. During our period of interest, they are usually without many gaps, except on the 13th to 17th of February. We use them qualitatively, so contamination by colored dissolved matter or particles is not an issue for the objectives of this study. Geostrophic current maps are produced by Ssalto/Duacs and distributed by Copernicus-Marine Environment Services (CMEMS). The currents are computed from absolute dynamical topography mapped using an optimal interpolation method

(Taburet et al., 2019). The maps (product SEALEVEL_GLO_PHY_L4_NRT_OBSERVATIONS_008_046) are produced daily on a $0.25^\circ \times 0.25^\circ$ grid, based on combined altimetric data of all the satellite missions within the time window from at least 15 days before to 6 days after the date of interest. Mean currents are added to the anomaly as described in Rio et al. (2011). The spatial scales resolved in the currents are usually on the order of 100 km or more, with significant damping at smaller scales (see also Dibarboure et al., 2011, for an earlier product).

The salinity products used are from the Soil Moisture Ocean Salinity (SMOS, January 2010–present), and Soil Moisture Active Passive (SMAP, April 2015–present) missions. The European-led SMOS and the NASA SMAP missions observe the surface by L-band radiometry from sun-synchronous polar-orbiting satellites (Entekhabi et al., 2010; Font et al., 2009; Kerr et al., 2010; Piepmeier et al., 2017; Reul et al., 2020). Both SMOS and SMAP orbits cover the entire globe within 3 days with data provided close to 6 a.m. and 6 p.m. local time. The retrieved SSS has a spatial resolution of ~ 45 km for SMOS and between ~ 40 and ~ 50 km for SMAP. Here, we use the SSS acquired each day on ascending and descending orbits separately, the SMOS L2Q fields (doi: <https://doi.org/10.12770/12dba510-cd71-4d4f-9fc1-9cc027d128b0>), corrected for systematic errors depending on the geometry of acquisition of the satellite (Boutin et al., 2018), delivered by Centre Aval de Traitement des Données (CATDS) and the SMAP L2 fields delivered by Remote Sensing System (RSS v4 40 km). The SMAP product is a little smoother than SMOS, and it generally has smaller errors also suggesting slightly larger scales resolved. Two SMOS images with evidence of Radio-frequency interference contamination have been removed during the period investigated, and the contamination became worse later in February. We also use SMOS and SMAP combined weekly SSS generated by the Climate Change Initiative Sea Surface Salinity (CCI + SSS) project (doi: <https://doi.org/10.5285/4ce685bff631459f-b2a30faa699f3fc5>). It provides weekly level-3 SSS data from 2010 to 2019 at a spatial resolution of 50 km, a sampling of 25 km and 1 day, by combining data from the SMOS, Aquarius, and SMAP missions.

We illustrate the different products on the 12th of February, when the fresh plume was fully developed along 56°W (Figure 3). Both SMAP and SMOS SSS show a mostly south-to-north structure along 56°W extending from the shelf over to the deep ocean (shelf break in white), although with a slightly different pattern (note that they are taken 12 h apart). The Chla map also shows filaments and regions of higher load, which could be either chlorophyll, remnants of Color Dissolved Organic Matter or remnants of sediment and detrital matter not fully filtered out of the products. These structures align to some extent with the currents that connect the outer area of the shelf to the deep ocean. They are located on the western side of a large anticyclonic eddy shed by the NBC retroflection (A1). A smaller cyclonic structure (C1) is also visible close to the shelf break, southwest of the northward currents. The Chla map presents finer scales, as expected from the better resolution of the satellite imagery in the visible part of the spectrum compared to L-band radiometry.

SMAP L2 and SMOS L2Q maps present systematic differences with respect to in situ data that also depend on whether they correspond to descending or ascending tracks. The issue is particularly large for the SMOS product where the systematic differences are also found to vary across the tracks, in particular on the eastern edge of the descending tracks due to a sun-tail contamination not filtered out in the L2Q fields. Part of this contamination is however taken into account in the estimated error provided with the SMOS L2Q products and we eliminated SMOS data for which the estimated error was larger than 1 pss. We attempted to correct the remaining systematic differences on a track by track basis, although the applied adjustment is often uncertain at the 0.1–0.2 pss level, in particular for SMOS. We did not correct island effects on the SMAP maps that are particularly noticeable to the east/north-east of islands (Grotsky et al., 2018) because they are mostly outside of the main area of our study.

In order to provide full salinity fields and reduce errors by averaging enough data, we combined the adjusted SMOS and SMAP L2 gridded fields. As the fresh plume evolves on a roughly daily time scale, as observed for example from Chla maps, it is best to keep a rather short time averaging. For half the days, combining the tracks at 6 a.m. and 6 p.m. (local time) was sufficient to provide full coverage of the fresh water plume. For other days, it was necessary to add data from 6 p.m. of the previous day (thus a total time span exceeding 24 h). This leaves only 2 days with no salinity product, out of the 20 days investigated.

At each grid point, the field value is estimated by a simple weighting of data inversely proportional to the L2Q estimated error, and with a spatial weight decaying as a Gaussian with a radius of 30 km as a function

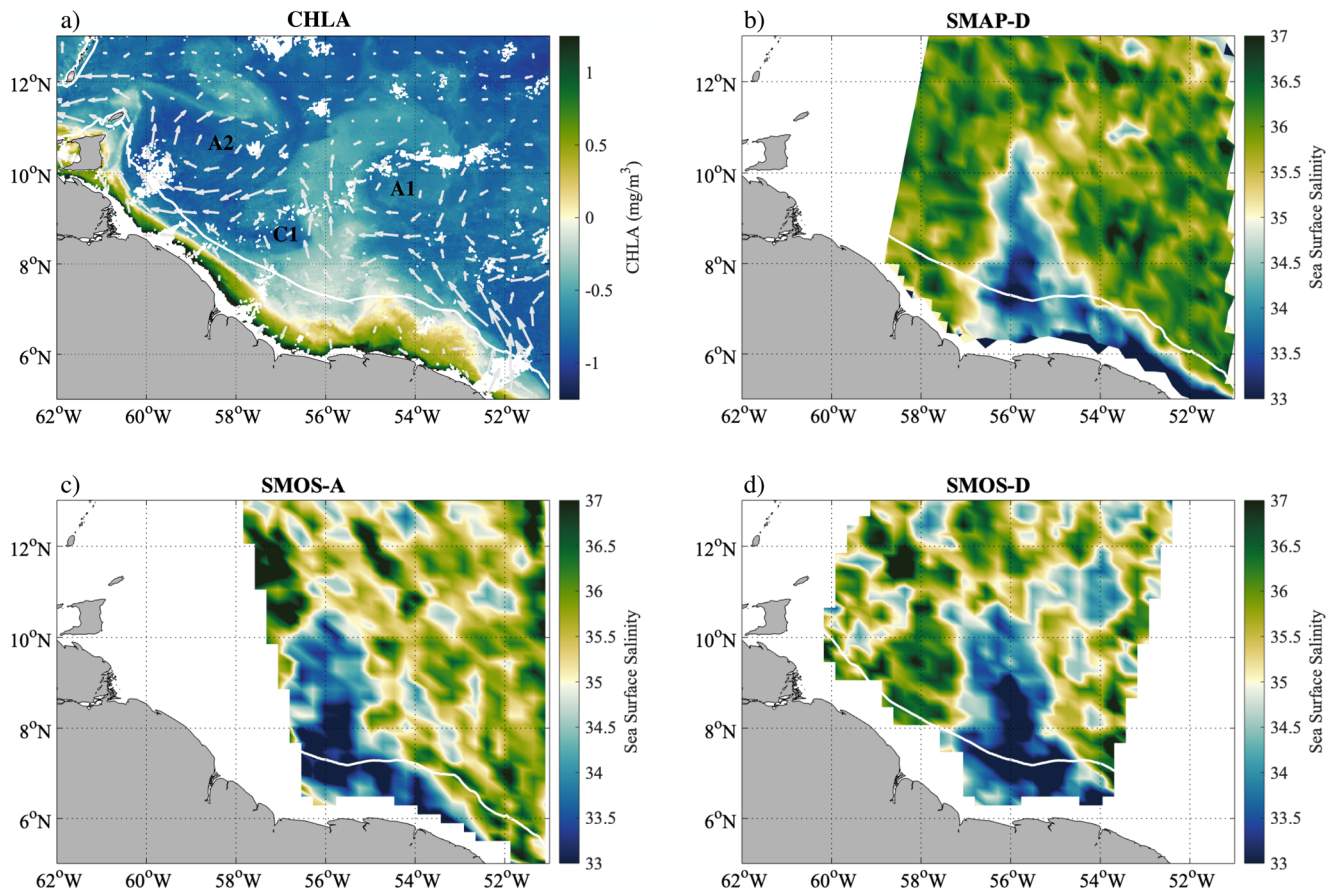


Figure 3. Satellite maps on February 12th. Chla and geostrophic currents (white arrows, a), SMAP SSS along its descending track (b), SMOS SSS along its ascending (c), and descending track (d) for the 12th of February. The shelf break is represented by the 100-m bathymetry contour (white line). Two anticyclonic (A1, A2) and one cyclonic (C1) eddy are labeled in (a).

of the distance of the data to the grid point. No data farther than 50 km is incorporated. We also assumed that errors on data closer than 25 km are fully correlated to account for the real footprint of the satellite data which is on the order of 50 km. The resolution of the final daily field is probably close to 70 km. Estimated uncertainties on the daily fields are typically on the order of 0.5 pss, consistent with the comparison to in situ data. The comparisons with in situ data also suggest that the daily fields tend to produce higher salinities in the core of the plume with the freshest observed salinities, and lower salinities on the sides. These are possible effects of the salinity field smoothing, although we could not fully verify it as data coverage was not evenly distributed. The daily fields nevertheless give precious information on the salinity distribution as illustrated in Figure 2 for the average over 18 days.

The IFREMER CERSAT Global Blended Mean Wind Fields product, distributed by CMEMS, is used in this study. It provides 6-hourly surface winds in the region of interest on a spatial grid of 0.25° in latitude and longitude. From 2010 to 2018, the reprocessed product is used (WIND_GLO_WIND_L4_REP_OBSERVATIONS_012_006), while for 2019 and 2020 we used the near real time one (WIND_GLO_WIND_L4_NRT_OBSERVATIONS_012_004).

Finally, we used ocean velocity and salinity outputs from the Mercator PSY2V4 model, both in analysis and forecast modes. These were made accessible, together with all satellite data, to guide the ships during the field campaign in order to survey the fresh water plumes (Figure 4). Since January 30th they consistently suggested a westward (and possibly offshore) extension of the eastern Guiana shelf fresh pool, although they sometimes missed the full extent of the plume's offshore extension.

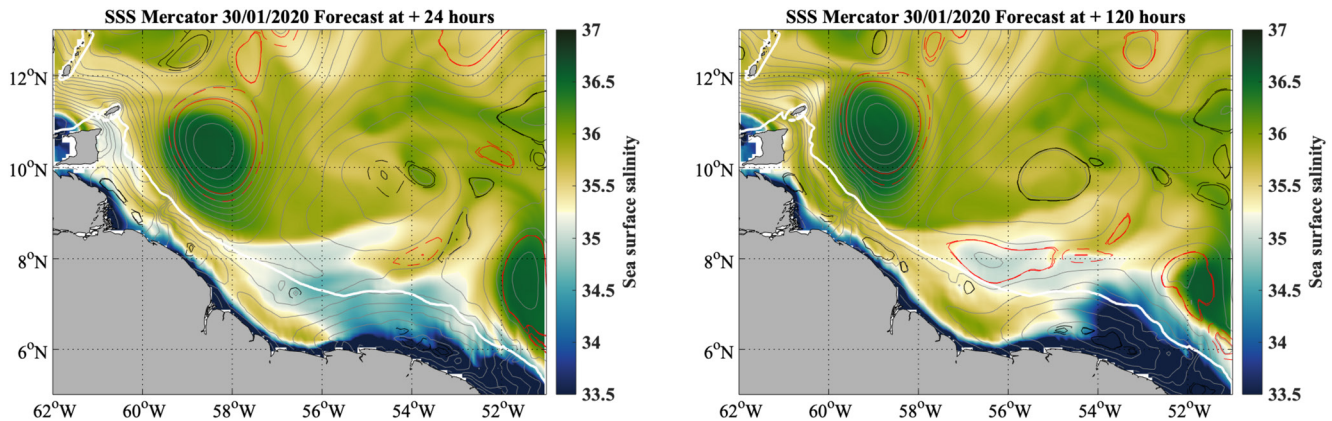


Figure 4. Mercator PSY2V4 model SSS (color) and sea level (gray contours) forecast and eddy detection made on the January 30, 2020 for January 31, 2020 (left) and February 4, 2020 (right). The eddy detection is shown by dashed contours (red for anticyclones and black for cyclones; Laxenaire et al., 2018). The shelf break is represented by the 100-m bathymetry contour (white line).

3. Results

3.1. Life of the Plume

In late January 2020, the region located between 7°N north of the continental shelves of the Guianas and up to 12°N is mostly covered by surface water with a salinity between 35 and 36.5 pss (Figure 4), which is typical in this season of low precipitation and low input of freshwater from the Amazon and Orinoco rivers (Figure 1). Freshwater is witnessed edging north-westward on the shelf east of French Guiana in late January, both in satellite products and in the Mercator PSY2V4 model simulations. Near 53°W, the shelf break bathymetry changes. Overall, the shallow isobaths tend to be zonally oriented west of 53°W, with a large cone (DR) associated with past sediment transport extending farther offshore and presenting less steep off-shelf topography. Changes in geostrophic currents, often associated with the retroflexion of the NBC and formation of anticyclonic eddies to the northeast of the cone, would favor near-surface northward transport. In addition, the wind direction being less orthogonal to bathymetry would also favor off-shelf Ekman transport. Off-shelf transport events are thus expected near that longitude.

Indeed, this is what was forecasted from the Mercator PSY2V4 operational model on January 30th with a clear off-shelf extension of the fresh pool indicated on February 4th, even though it did not extend as a full-fledged plume (Figure 4). Three SVP drifters were released into this freshened plume on February 2nd, and two additional drifters were deployed during a return section of RV *Atalante* on the 4th–5th of February a little further north, as the plume extended in that direction (with salinity dropping across this section to close to 30 pss) (Figure 2).

To illustrate the plume evolution, we present (Figure 5) daily snapshots of *Chla* and sea surface salinity. The freshwater off-shore event started on February 4th, when the plume began to detach from the shelf, overflowing the shelf break near 53°W–54°W. An anticyclonic NBC ring (A1) northeast of the plume had already entrained relatively fresh water (SSS on the order of 35 pss) since late January all the way up to 10°N. This feature is also seen on the *Chla* distribution across the shelf break. The northward offshore transport of fresh and productive water continued on the 7th of February, following fairly well the surface geostrophic currents. The anticyclonic eddy (A1) centered around 54.5°W–9.5°N likely participated in advecting water from the plume northward (on its western side) and limited its westward propagation. A small cyclonic eddy (56.5°W–8°N, C1) channeled the northward geostrophic flow and also contributed in steering the plume northward. The situation was quite similar on the 9th and on the 12th with the northernmost part of the plume, rich in chlorophyll, steered by the northern part of the anticyclonic eddy A1. In the meantime, the plume started to be influenced to its west by the eastern side of a second anticyclonic eddy (A2, centered around 58.5°W–11°N). Around the 12th, we observe the first indication (in particular in SSS) suggesting a future separation of the plume from the shelf. This separation started on the 14th of February and was clearly visible on the 15th. The dynamic situation changed quickly as the cyclonic eddy C1 disappeared,

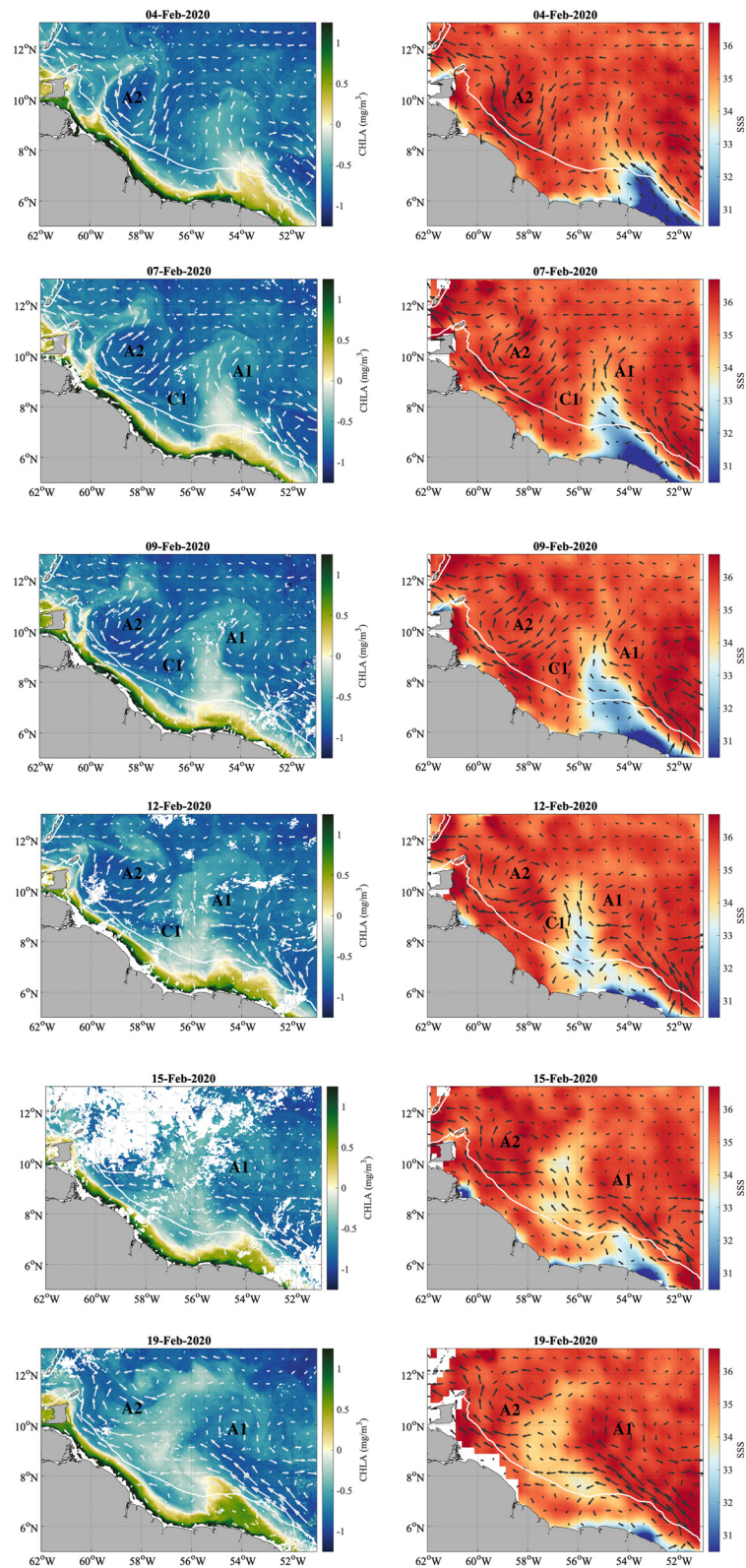


Figure 5. Snapshots of daily satellite Chl *a* and SSS maps with overlaid geostrophic currents (arrows) for the 4th, 7th, 9th, 12th, 15th, and 19th of February 2020. The shelf break is represented by the 100-m bathymetry contour (white line).

with a strong north-westward current near the shelf almost topographically steered, and the two anticyclones north of 9°N. The fresh pool formed by the plume spread horizontally (and probably vertically), with surface salinity on the order of 33.5–34 pss.

Intrusion of salty water from farther west near 9°N might have contributed to the erosion of the salinity minimum. This is particularly pronounced on the February 15th map. At that date, two drifters close together experienced very large salinity differences (up to 0.5 pss at 3-km distance near 9°N/56.6°W), illustrating how sharp the gradients were near this wedge of salty and low Chl a water. Horizontal mixing with the plume water can be expected from this date, except if the saltier/Chl a -free water is entrained under the fresher water. This penetrating saltier water seems to partially separate fresher water to the north from the freshwater closer to the shelves.

On the 17th and 18th of February, the Saildrone crossing the fresh pool still encountered SSS as low as 33.3 pss near 9.8°N/56.5°W, similar to what is suggested by the salinity maps (Figures 2 and 5). Then, by February 19th, the low salinity pool had become less pronounced (minimum values increase to 34 pss), but had extended further westward in particular just north of the shelf break, nearly reaching the southern edge of eddy A2. Afterward, it was difficult to follow because of uncertainties in the salinity maps that are on the order of 0.5 pss.

Another way to investigate the plume evolution is to consider a Lagrangian perspective, based on the time series of the five drifters deployed in the plume (SSS lower than 35 pss) on February 2nd and 4th either on the shelf or near the shelf break. For the first 4–5 days after deployment they drifted north to north-westward and remained coherently separated cross-stream (Figure 6a). The drifters are drogued at 15-m depth, which might be within the stratified layer under the freshest surface water, in particular at deployment (see Section 3.2). The drifters were deployed in a horizontal gradient of SST (1°C change across the plume), with coldest water closest to the continent. Interestingly, this gradient as observed by the drifters remained fairly consistent over time, although its amplitude gradually diminished (Figure 6b). Moreover, large temperature daily cycles are observed, with initial amplitude exceeding 0.5°C. The wind (Figure 6d) also illustrates a daily cycle with strongest wind in the early morning and weakest wind in the late afternoon. It was relatively weaker at the beginning of the deployment near the shelf break, in line with the corresponding larger temperature daily cycle. For all drifters the wind increased over time during this initial 5-day period and as the drifters moved away from the shelf.

Salinity (Figure 6c) variability between the different trajectories is not as regular as temperature variability. The trajectories present some rather fast changes of SSS (by up to 1 pss), which indicate the presence of small-scale gradients/blobs advected relative to the drifters. The red salinity curve, corresponding to one of the middle deployments, remained the lowest. Nevertheless, 7 days after its deployment, it has values very close to the black curve (corresponding to a drifter located to its northeast, in slightly warmer water). It is the drifter farthest east (gray line, always off shelf) that presents the least variability. All together during this period and for all drifters, salinity is very similar at 0.20-m and 5-m depths whereas there are gradients of up to 1 pss between the surface and 10 m for most drifters (Figure 6e). This is not found for the drifter that is farthest from the shelf (gray curve). It indicates a deeper fresh layer in this region, even though at times this drifter presents lower salinity than the drifter closest to shore (green curve). The periods of large salinity stratification between the surface and 10 m depth are not found at the same times for the different drifters (Figure 6e). They tend to be less common on February 6th and 7th, after a few days of drift away from the shelf and with the stronger winds.

3.2. Sections Across the Plume (Extension, Gradients, and Thickness)

On the 2nd of February both RV Atalante and MSM crossed the nascent plume (Figure 7a). The overall currents were directed to the northwest, so in general the MSM section is upstream from the Atalante sections. Both vessels were coming from the deep ocean over the outer shelf, with salinity decreasing and reaching a plateau, until a sharp front was encountered by the two ships. This front is located on the shelf near 06.68°N/53.51°W (Atalante) and 06.78°N/53.25°W (MSM), with much fresher (by more than 1.2 pss) and warmer water on the inner-shelf side of the front (Figure 7b with the inner-shelf to the left and values on the x -axis increasing offshore). Interestingly, the front was farther away from the coast and with warmer

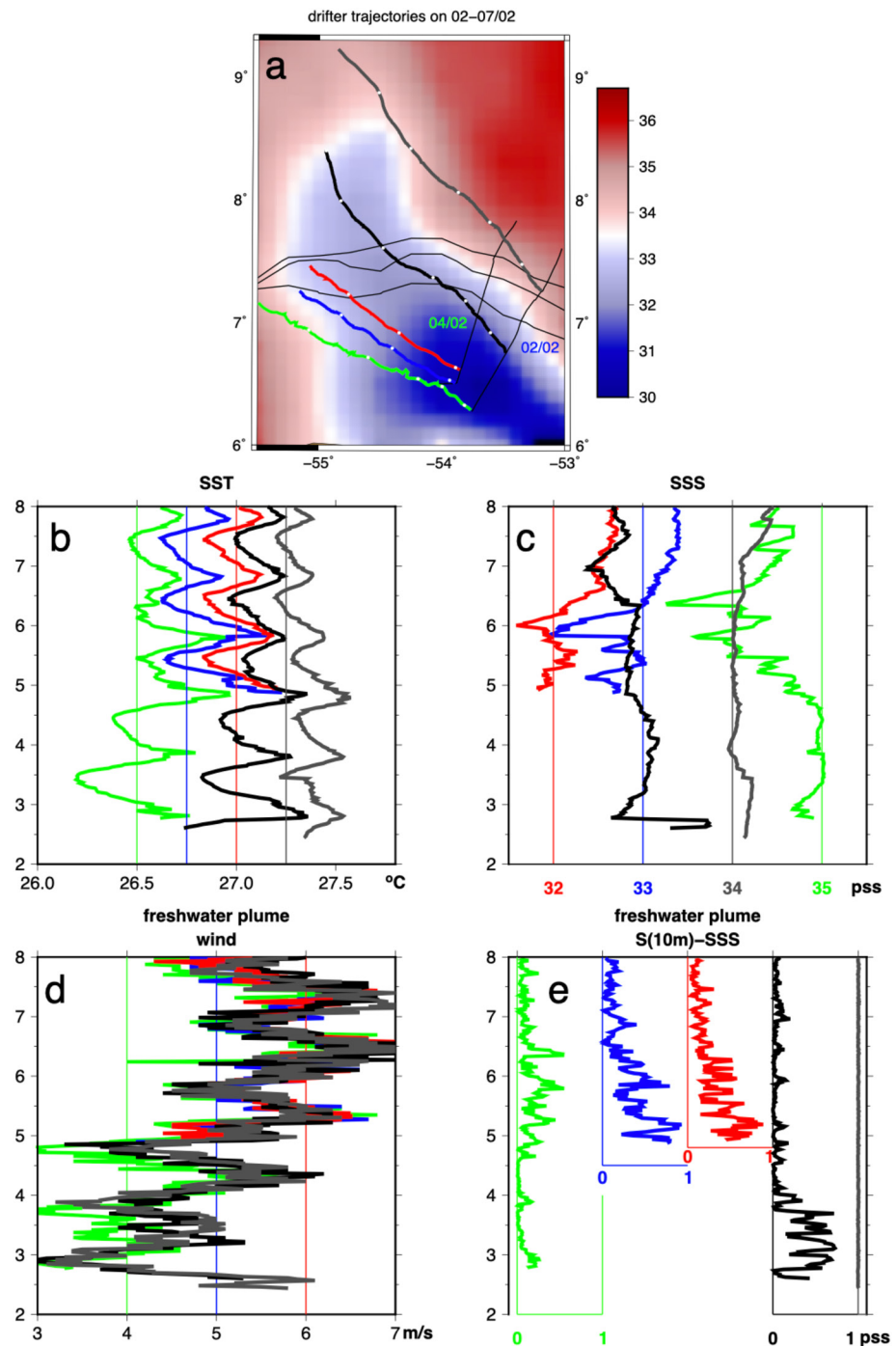


Figure 6. The drifter time series from February 2nd to 7th. Top panel, the trajectories (with dots each day at 0 GMT), as well as the SSS map for February 7. Below, four panels as a function of time (vertical axis in February days) for sea surface temperature (b, top left), sea surface salinity (c, top right), measured winds (d, bottom left in m/s), and salinity stratification $S(10\text{ m})-S(0.2\text{ m})$ (e, lower right). The curves are color-coded for the different drifters based on panel (a) (panel (e), the colored vertical straight lines correspond to no-stratification for that drifter).

and fresher water on its southwest side for the MSM section compared to the Atalante section (Figure 7b). The surface front width is crossed in less than 100 m based on the RV Atalante intake temperature sensor measurements, and is possibly as narrow as 50 m. The respective positions of the front crossings by the two vessels suggest that the front was oriented northeast to southwest. The lower SSS seen by MSM suggests

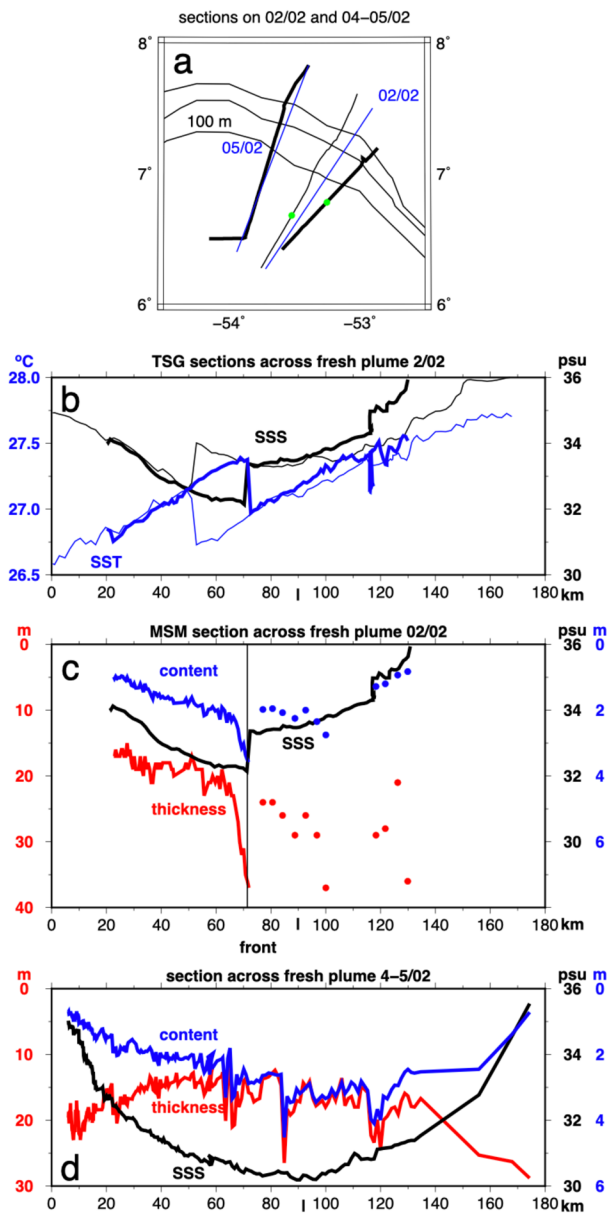


Figure 7. Sections across the shelf break near 53°W-54°W. (a) (top panel) Map with the different sections (thin black line for RV Atalante on February 2nd, and thick black line for Maria S. Merian (MSM) on February 2nd and RV Atalante on 4th–5th). The blue lines indicate the axis along which the data are projected for the plots (the 100-, 300-, and 500-m isobaths are plotted), and the green dots indicate the positions of a T/S front. (b) Sea surface temperature (SST) (blue) and SSS (black) sections on 2nd of February from RV Atalante (thin) and MSM (thick) transects. The horizontal axis is distance from the end point on the shelf (53.72°W/6.27°N) and the data of the two ships are projected on the same line median to the two ship tracks. (c and d) Lower panels: the moving vessel profiler (MVP) sections on 2/02 (MSM) and 4–5/02 (RV Atalante) plotted for SSS (black), fresh layer thickness (red) and equivalent freshwater content (blue), with respect to distance from its origin on the shelf (at distances larger than 75 km/134 km on (c)/(d)), uCTD profiles instead of MVP data. The vertical bar on bottom axis on both panels indicates the location of the 100-m isobath. For (c), the position of the sharp front in SSS/SST is noted by a vertical line.

that the front might have been propagating from southeast to northwest, as fresher water was found farther upstream along the shelf break and shelf (i.e., farther southeast) according to the salinity satellite maps and the Mercator PSY2V4 operation model. Indeed, it is probably the same sharp front that was crossed by one drifter (black line in Figure 6c with more than 1 psu drop and 0.4 C warming in an hour) less than 4 h after its deployment from RV Atalante. As it is located a little to the north of the position of the front crossed by RV Atalante, it suggests that the drifter was also encountering freshwater coming from its east or southeast.

The combined MVP and uCTD section collected by MSM on February 2nd (note that the MVP started just after crossing the surface front) will be summarized by presenting the thickness of the freshwater plume and equivalent fresh water content (cf. salinity section in supporting information S4). The thickness of the freshwater plume (red curve in Figure 7c) is defined here by the depth where salinity reaches $0.5 \cdot (36.4 + \text{SSS})$ corresponding to surface and subsurface waters that have been equally mixed assuming homogeneous salinity profiles above and just below this depth. Here 36.4 psu is a typical value of salinity near 50 m in this survey. The equivalent fresh water content is estimated by vertically integrating the salinity profiles assuming mixing of fresh water with salty water at 36.4 psu. The thickness of the fresh layer and the equivalent freshwater content (referred to 36.4 psu) present strong variability across the section (Figure 7c). In particular, there is a large bulge in the freshwater layer thickness just inshore (left on Figure 7c) from the front. Indeed, in this bulge, the very fresh surface water presents stratified salinity down from the near-surface to 40-m depth, with water properties at 22 m corresponding to those in the surface water found northeast of the front (cf., supporting information S4). This suggests that the freshest surface water had recently overlaid the saltier/warmer water, which had downwelled under the front. Farther to the northeast along that section, there is only a slight decrease of the fresh water content (blue curve on Figure 7d) due to deeper surface mixed layer despite higher surface salinity (black curve on Figures 7c and 7d), especially east of the shelf break (but the number of profiles collected is insufficient to fully apprehend this structure).

On the 4th and 5th of February, RV Atalante crossed the fresh plume on its way from the shelf to the southern side of anticyclonic eddy A1 of Figure 5, a little bit to the west of the earlier crossings (Figure 7a). Salinity dropped to nearly 30 psu close to the outer edge of the shelf (Figure 7d) and presents very regular and symmetric along-track variability relative to the shelf edge, with no trace of the earlier fronts witnessed on February 2nd. This suggests that at that time the plume was rather broad and at least 120 km across, assuming that the section was at a right angle to it. This assumption about the angle (maybe closer to 70°) is supported by the salinity maps, the drifter trajectories and the ship's vessel mounted ADCP (VM-ADCP), which suggest that the upper ocean currents were nearly at right angles to the cruise track.

On February 5th the MVP (and uCTD) profiles also provide information on the plume's vertical structure (Figure 7d). Based on the salinity criteria for the fresh layer thickness, the section presents thicker fresh layers on the sides of the plume than in between, where it is typically 12–20-m thick (red curve). The fresh layer thickness also presents some very fast variability between successive profiles, for example at 65, 83, and near

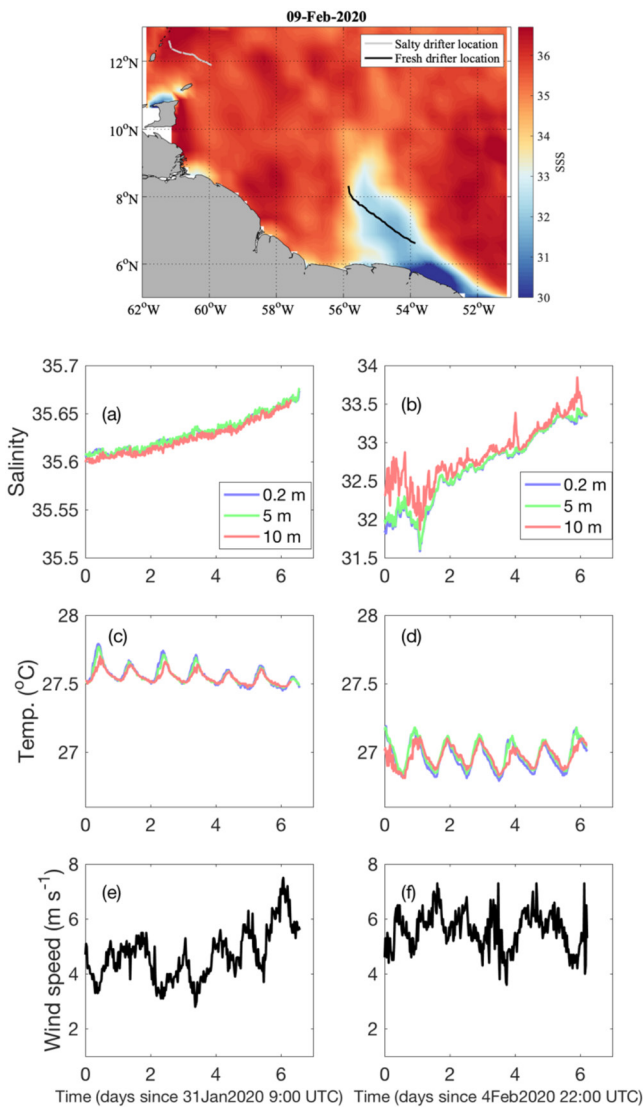


Figure 8. Salty (light gray) and fresh (dark) drifter trajectories are overlaid on the salinity map for February 9 (g, top map). Under it, comparative time series for (left column) the drifter deployed in salty water (on January 31 at 09 GMT) and (right column) the one in fresher water (on February 2 at 22 GMT). Top panels for temperature measurements at 0.2, 5, and 10 m; middle panel for the salinity at these three levels, and bottom panel wind measurements.

120 km. This could be indicative of internal waves or solitons, and there are no associated surface salinity or temperature variations. The equivalent freshwater content is on the order of 2–4 m in the central outer parts of the plume, whereas it decreases a little more toward the shelf edge of the plume.

3.3. Stratification and Shear in the Surface Layer

The MVP sections performed close to the time when the plume separated from the shelf indicate that the fresh layer was rather shallow. We will present evidence of how this stratification constrains vertical mixing and the extent to which off-shore changes in the salinity plume are related to vertical mixing with the deeper saltier water.

The drifters show variable salinity stratification between the surface and 10-m depth in the first 5 days (Figure 6e). Such stratification is less common afterward, but some of the drifters also left the core of the fresh plume. Drifters launched in January stayed out of the fresher water region and can be compared with those launched in the plume in order to identify the characteristics of this surface layer. Such an example is presented in Figure 8, and although some differences might be related to weather conditions, such as different cloudiness, there are major differences between the drifter data in the plume and outside of the plume that we will describe. First, the temperature diurnal cycle is present in both the salty and fresh regions at the three depth levels but with strikingly different amplitudes (Figure 8). The larger diurnal cycle is observed for the buoy located in the freshwater plume despite experiencing winds that were often larger than for the out-of-the-plume drifter. At night in the freshwater plume, temperature remains a little warmer at 10-m depth than at the surface. Ten-meter temperature however usually decreases during night-time, which suggests active night-time vertical mixing near the surface entraining the 10-m subsurface water. Furthermore, surface salinity increases similarly during day and night-time in the salty region, whereas the increase is observed with more diurnal variations in the fresh plume. Except for an event on the second day (Figure 8), this seems to confirm the night entrainment of subsurface (salty) water into the near surface layer resulting in a late-night relative surface salinity maximum.

The records of the drifter data in the fresh plume therefore suggest night-time active mixing in the stratified layer near 10-m depth, just below the well-mixed surface layer. We do not have direct information of turbulence activity at that time. However, there is indirect evidence provided by the Ocarina platform deployment over the shelf on February 3rd (supporting information S1). As the local depth was larger than 50 m, interaction of the surface mixed layer with the deep boundary layer should have been

small. Nearby MVP profiles collected by RV Atalante (for density profiles) are combined with the simultaneous Ocarina current data (for shear) to estimate a Richardson number (R_i) profile (supporting information S1), with R_i defined as:

$$R_i = -g / \rho * (d\rho / dz) / \text{shear}^2$$

R_i has values between 0.2 and 0.8 in the 6–16-m layer. As the profiles were not exactly simultaneous in space and time, we cannot estimate individual R_i profiles and derive precise statistics on the R_i distribution, although the average is on the order of 0.4. These averaged values suggest that the whole layer might have witnessed active turbulent conditions, with values close to the critical R_i for shear-induced instability

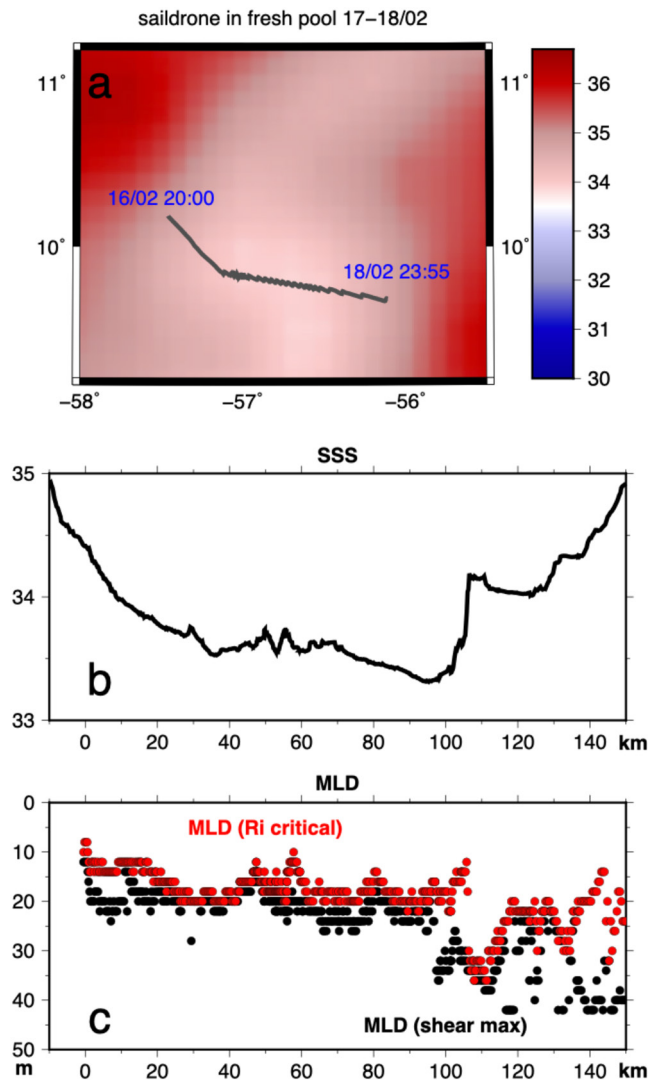


Figure 9. Saildrone section (16/02 evening to 18/02) across the fresh plume. (a) Track overlaid on the sea surface salinity (SSS) map for February 17; (b) SSS; (c) different estimates of MLD (maximum shear depth in black and from critical R_i number in red). (b) and (c) Plotted along the section from west to east, as a function of distance from an entrance point in the fresh pool.

(Galperin et al., 2007). This happened despite the stratification induced by daily heating, found at least between 6 and 14 m (15 m coincides with the lowest temperature in the profiles).

The Saildrone crossed the fresh pool two weeks later than the ship on the 17th and 18th of February (Figure 9a). They did not measure stratification directly, but the ADCP data at 2-m resolution can be used to estimate a mixing depth. This is done by assuming $R_i = 0.4$ in this layer, and then estimating the density profile in the actively mixed layer by vertically integrating $R_i \cdot \text{shear}^2 \cdot \frac{\rho}{g}$ down from the surface. The bottom depth of this layer (mixing depth) is reached when the density has increased relatively to the surface by 0.12 kg/m^3 (Foltz et al., 2018). Alternatively, we use the current profiles to identify the depth of maximum shear. This depth is known to be deeper than the mixing depth, either because of internal waves under the base of the mixed layer or the wind momentum input into the surface layer (Foltz et al., 2020). The two estimates of the mixing depth are quite similar, with the one based on maximum shear being deeper by about 9 m on average. They are weakly correlated (0.42) over the crossing of waters with salinity less than 34 pss (Figures 9b and 9c). The low correlation results from a small area near 100 km where the maximum shear is found deeper than mixed layer depth MLD based on critical R_i . Both estimates usually illustrate rather shallow mixed layers, often on the order of 20-m thick (averaging 17 m for the density criterion). The estimate is deeper in the eastern part after the sharp salinity frontal increase to 34.05 pss, where the two depths are closer to 30–40 m, which is more typical of what was found during the EUREC4A-OA surveys, at least at night time.

So, overall, MLDs (and presumably the freshwater layer thickness) in the plume are larger, possibly by close to 10 m, than what is observed on the sections 2 weeks earlier and closer to the shelf. There is also no clear diurnal cycle of the MLD within the plume, based on this indirect estimation (the freshest part of the plume was crossed in more than 1 day). This fits with the expectation that density stratification under sustained winds is constrained by the salinity stratification in these shallow and fresh surface layers. Interestingly, the width of the plume did not change much between February 2 (Figure 6) and February 18. On the other hand, it expanded northward significantly based on the satellite maps (Figure 4), extending to close to 12°N and becoming less linear. Minimum salinities reached in the plume are also larger by February 18.

3.4. Advective Budget for the Surface Area

To determine the causes of the freshwater plume's expansion, first we estimate the freshwater pool area from mapped satellite SSS daily products. We define it as the area bounded by the 35 pss isohaline and offshore of the 100-m isobath. We also estimate an advective area flux based on the currents across the shelf in sectors with salinity less than 35 pss. Currents are estimated by combining AVISO geostrophic currents and Ekman currents estimated with a mixing depth of 20 m and using wind stress estimates from the drifter closest to the shelf break. Note that 20 m is typical of the fresh layer thickness from the sections on the 2nd, 4th, and 5th of February (Figures 7c and 7d), but that is larger than the near 10-m MLD found on the southern part of those sections. It is also typical of the MLD observed by the Saildrone section of February 17 (Figure 9). The rate of change of the area should equal the area transport, assuming 2-D dynamics, no effect of mixing on this area, and conservation of SSS (no air-sea exchange of water).

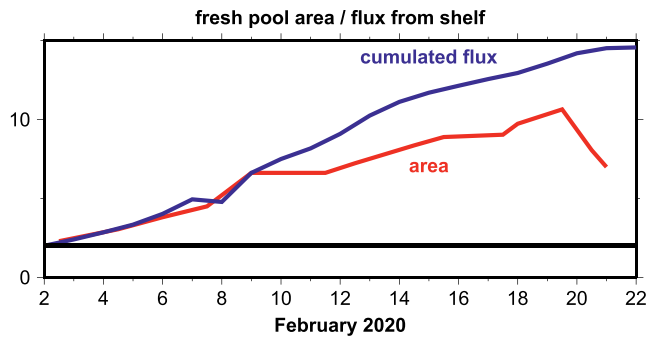


Figure 10. The area of the deep ocean sector with $S < 35$ pss and with depth larger than 100-m (in red; area expressed in 10^4 km²); the cumulated flux is the horizontal area with $S < 35$ pss fed by advection from the shelf, estimated assuming horizontal dynamics, no mixing and conservation of surface salinity (in blue).

The two terms are comparable, although there is often a smaller area increase compared to the flux. The area of the freshwater plume increases rapidly from the 2nd to the 9th of February (Figure 10) before increasing more slowly until the 19th and reaching a maximum of close to 100,000 km². For the fluxes, the increase is fast until the 14th of February and a bit slower until the 20th. As commented earlier on the plume history (Section 3.1), starting on 13th to 14th of February (Figure 3), there are some signs of partial separation of the fresh water plume from the shelf (and thus, some plume discontinuity). Interestingly the total area transport was driven almost equally by Ekman and geostrophic advection until the eleventh, and more by Ekman advection afterward.

We have estimated the total freshwater transport based on ocean currents and the surface salinity maps, though this might be less precise compared to the area transport. We use a constant freshwater layer thickness of 20 m based on the initial sections (Figure 7), and mixing with a 36.5 pss deep source. With these assumptions, we find that the transport of freshwater in this off-shelf plume averaged 0.15 Sv (10^6 m³ s⁻¹) in the 11 days from February 2nd to 11th, and 0.06 Sv from the 11th to the 20th. During

the first period, the transport is comparable to the expected outflow of the Amazon River in late January (based on climatology).

Until now, we have not commented on the uncertainties of these estimates. In supporting information S2, we estimate that uncertainties on the cumulative fluxes (blue curve on Figure 10) are between 15% and 50% (depending on whether or not the error is random in the daily flux estimates), whereas the error on the total area is likely to be on the order of 10%.

The difference between the two curves in Figure 10 is therefore probably within the error bars. Some of the assumptions done for this budget might also break down. Vertical mixing might diminish the area by bringing more salty water and causing mixed layer salinity to rise above the threshold in some areas (there is evidence of mixed layer deepening in the Sairdrone section on February 17th and 18th). There are also clearly some lateral intrusions/mixing with saltier water, but how this affects the overall area is not straightforward. These issues will be more easily addressed in high resolution numerical simulations and a full three-dimensional budget, as the salinity fields clearly do not have the required resolution for these mesoscale or sub-mesoscale features).

It is even more uncertain to provide an estimate of the total freshwater transport, as the freshwater thickness is not closely correlated with surface salinity, as illustrated in Figure 7.

4. Discussion

4.1. Frequency of Such Freshwater Plumes

How often do these freshwater events occur in the winter season during the January to mid-March period, and what drives them? Using the 10 years of weekly CCI SSS products, in each year we find events of freshwater leaving the shelf and reaching the open ocean. Some events happened farther west, west of 56°W and in some cases the fresh water did not extend north of 10°N. These events (two thirds of the total) were unlikely to have a lasting influence in this sector of the Atlantic, with the freshwater being quickly washed across the Antilles into the Caribbean Sea. Events closer to the one observed in early February 2020 happened in 7 out of 10 years during the winter season (supporting information S3).

An important question is what determines the presence or absence of off-shelf transport of fresher water. A requirement is that freshwater has to be transported from the Amazon estuary near the equator to 7°N/54°W. At this place, the shelf-break direction changes and winds become less perpendicular to bathymetry and thus prone to induce off-shelf transport. Southeast of that, the winds tend to be perpendicular to the shelf break, and even oriented a little farther anti-clockwise in January-February. This, close to the equator, does not favor the north-westward transport of freshwater on the shelf.

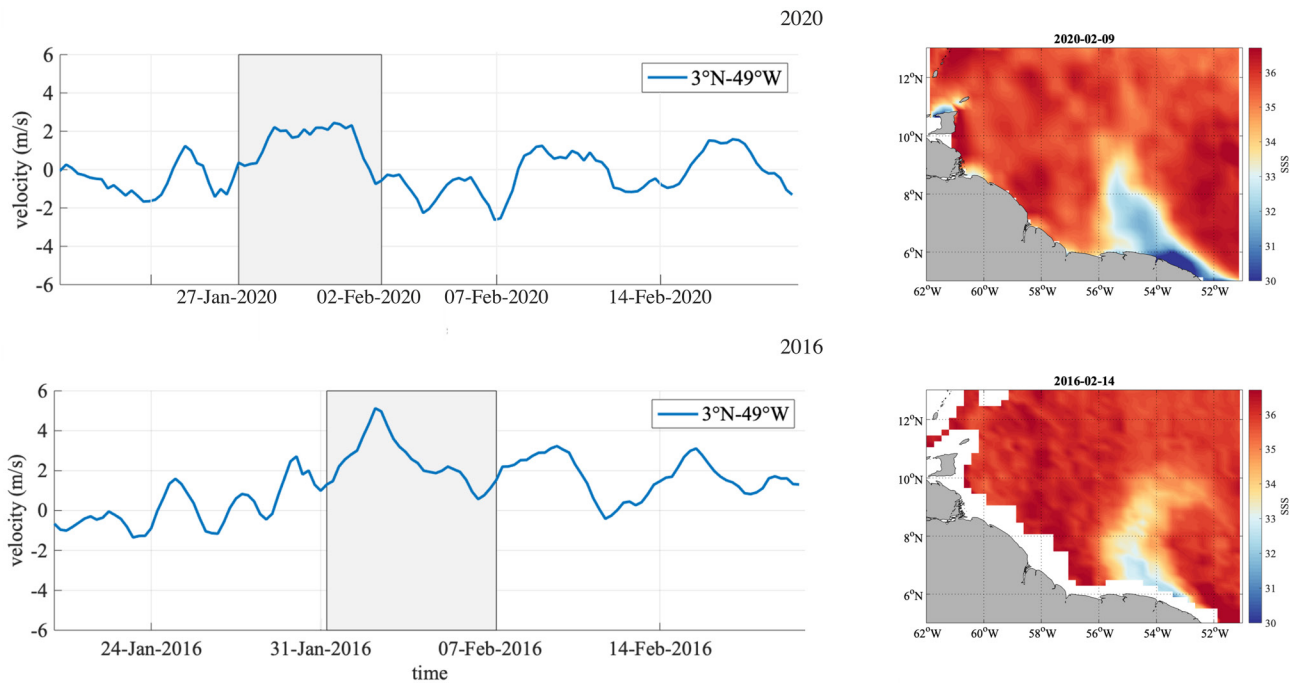


Figure 11. Winds at 3°N/49°W in relation to development of freshwater plume events. Only the component of the wind parallel to 100-m isobath is shown on left side for two years (2020, the event we study here; and 2016, a typical other year), with the corresponding developed freshwater plumes presented on the right side (for 2016, from CCI 7-day products). The gray time domain on the wind time series corresponds to the period between the start of the wind event and the start of the freshwater plume separation from the shelf near 54°W-56°W.

Small changes of wind direction are instrumental in inducing northwestward transport of Amazon water on the shelf (Geyer et al., 1991; Lentz, 1995). To estimate when this happens, we define an index based on the wind component parallel to the shelf-break at 3°N, a transition latitude with respect to the Coriolis force. It is halfway along the shelf between the Amazon estuary and French Guiana and is almost always bathed in freshwater. The index is the deviation of the wind component parallel to the shelf break from its average during the months of January and February of that year (positive to the northwest). In 2020, between mid-January to late February, we find only one 4-day period (January 28 to February 1) when the index is positive (Figure 11). This change in wind direction is favorable for a north-westward transport of freshwater which, if it flows at 50 cm/s, a typical along-shelf velocity in this season (Geyer et al., 1991; Lentz, 1995) would reach the shelf-break near 53°W-54°W in early February. The timing is thus fairly close to what is observed.

We cannot carry out such a detailed calculation in other years, as we do not know the precise date of appearance of the freshwater plume. However, we find that in 6 out of the 7 years when a freshwater plume developed (the exception being 2018), there was a preceding period with significant positive wind index lasting for a few days. An example is presented in the lower panels of Figure 11. The average length of these positive index events is 5.3 days (varying between 2 and 8.5 days), and the duration between the initial date of the wind event and the development of the off-shelf freshwater plume is 6.3 days (varying between 4 and 9 days). These estimates are in the range of what we expect for wind-induced currents. The time scales are long enough that geostrophy and Ekman divergence at the coast might be operating, which would reinforce the north-westward geostrophic current. Of course, other dynamics such as those associated with the shelf-break currents, or the build-up of a pressure head and its evolution near the mouth of the Amazon estuary might also take place.

Another key feature favoring the transport of the plume off the shelf is the anticyclonic eddy (A1) with a core lying slightly east of 54°W. This is an area commonly crossed by NBC rings (Johns et al., 2003). In 2020, the analysis of eddy A1 shows that it did not move very swiftly north-westward before February 21 (Figure 12). In particular, between February 7 and 14, the core stalled and only marginally moved to the

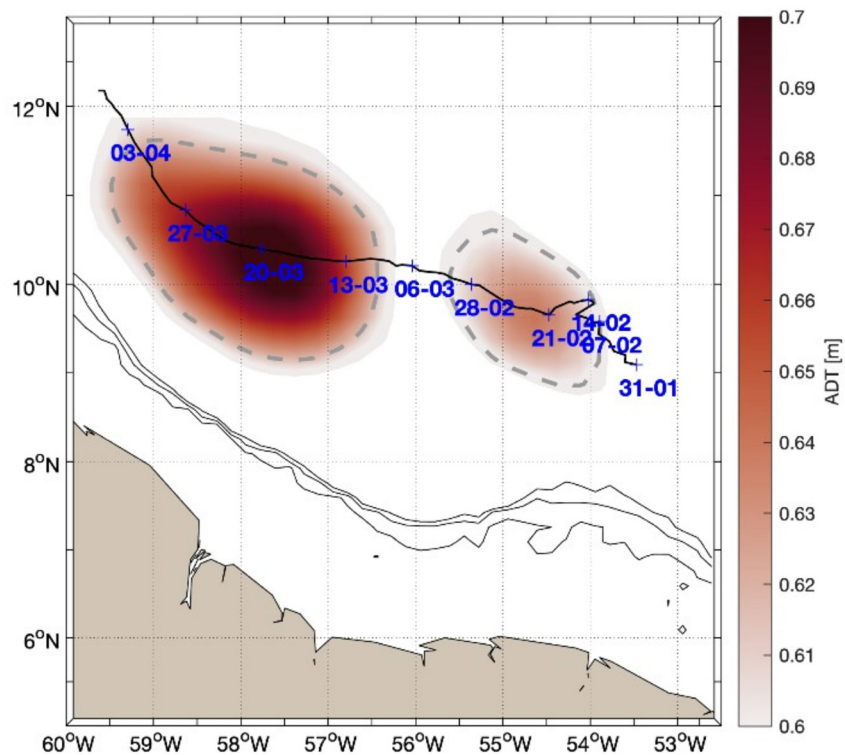


Figure 12. Trajectory of anticyclone A1 derived from absolute dynamical topography (ADT) maps by the TOEddies algorithm (Laxenaire et al., 2018). Composite ADT signature of A1 are indicated for February 23 and March 21. The shelf break is represented by the 100-, 300-, and 500-m bathymetry contours (black lines).

north, while separating from the shelf-break. This slow motion and the earlier presence of cyclonic feature C1 favors the channeling of the fresh plume by the geostrophic flow from the shelf-break farther north. At the same time, C1 weakens, and A2, another anticyclonic feature farther west moves slowly westward until mid-February, leaving a large area for the plume spreading. Then A1 rapidly moves farther west and intensifies, which would channel a large part of the fresh water closer to the shelf break near Trinidad toward the Antilles (Figure 12), as is suggested by the drifters and later weekly salinity maps.

4.2. Sharp Fronts

The daily salinity composite fields have a resolution on the order of 70 km, whereas the daily composites for Chla have a resolution slightly blurred by the compositing (for example a feature moving at 30 cm/s will be displaced by 26 km in 1 day), and the geostrophic current maps do not resolve structures with diameters smaller than 150 km, implying a large time averaging. Much finer fronts are features common in the surveys (for example in Figures 7 and 9). Some of these fronts have very large amplitudes, comparable to the mesoscales and are associated with strong surface density changes, and thus are dynamically active. The best resolved structure is the one crossed by two research vessels and one drifter on February 2nd (Figure 7). The intake temperature record of RV Atalante suggests a horizontal scale of the SST and SSS front of less than 100 m and possibly as short as 50 m. According to the VM-ADCP data of the two vessels, this surface front was embedded in a wider and deeper current pointing north-westward. However, data also suggest a rather narrow surface velocity structure just south of the front, with a sharp change of velocity at the sea surface front.

For instance, the RV Atalante absolute velocity presents a westward velocity peak of close to 30 cm/s at the front relative to the velocity before and after the front, despite the ship navigating at a constant speed relative to the sea surface. This peak velocity lasts less than 3 min, thus over a rather small distance of less than 1 km. There is also some indication of a change in the meridional velocity across the front, with the

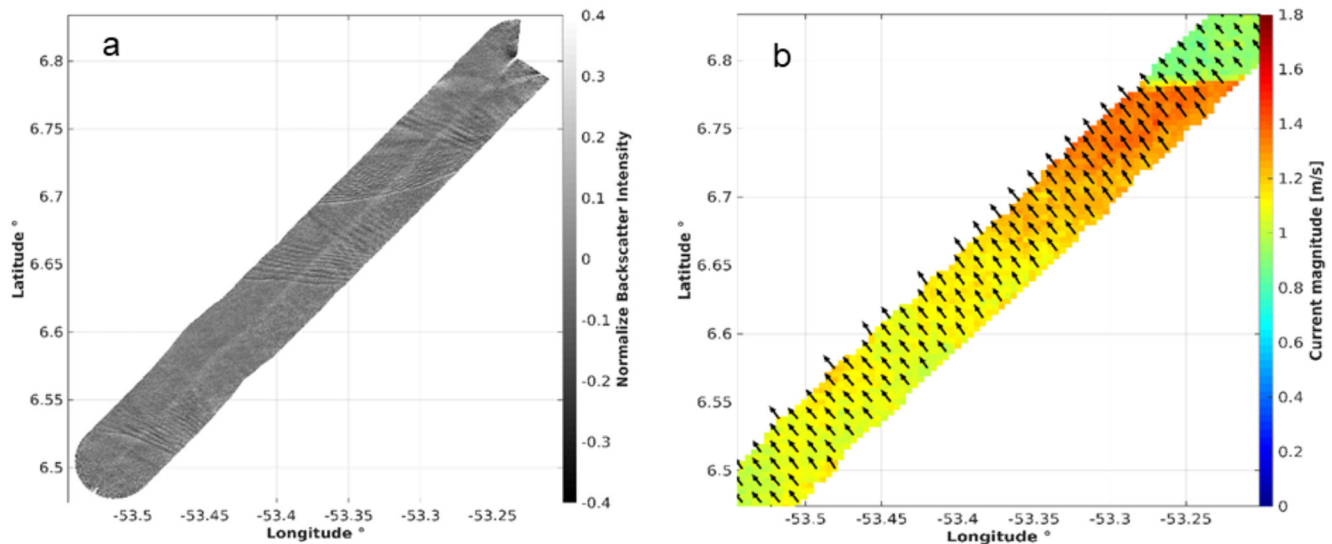


Figure 13. Marine radar data between 14:03 and 17:42 on February 2, 2020. Left panel shows backscatter intensity, whereas right panel shows retrieved surface currents, both as arrows and color-coded. The surface front was observed in T-S close to the north-east corner of the plots near $-53.25^{\circ}\text{W}/6.78^{\circ}\text{N}$.

surface velocity directed more northward south of the front than north of the front. On the MSM VM-ADCP shallowest bin at 18-m depth, the velocity vectors also suggest that the structure is converging at least in the direction of the ship's track. There is also a westward narrow velocity peak of 25 cm/s over less than 7 km relative to velocities further away. However, because of the large salinity bulge southwest of the front (Figure 7c) under the lowest surface salinity, these velocity structures at 18 m are difficult to interpret, as the uppermost ADCP bin is within the fresher layer close to and southwest of the front, whereas it is in the saltier water under it in other areas. Fortunately, there is also the evidence from the MR radar surface data (Figure 13).

As the normalized backscatter intensity is strongly dependent on the ocean surface roughness it depicts all structures that affect the surface roughness, including several internal wave packets along the track, as well as the strong current front close to the northeast corner of the plot. During the 3:39 h track plotted, the surface currents (top 5 m) are pointing northwestward with an increase of velocity along the track toward the northeast, until the velocity front is encountered at the same location as the SST/SSS front. The velocity front at 6.78°N is almost zonal with a slight southward tilt toward the west, and it is associated with a sharp current jump of ~ 0.5 m/s.

The drifter that crossed the front (farther west and a few hours later) also shows a 50 cm/s westward velocity surge near the front. This surge lasted over 2.5 h, longer than the change in surface temperature and salinity that lasted less than 1 h. It is difficult to translate that into a horizontal scale of the current feature, as it would involve knowing the velocity of the front relative to the drifter. Also, notice that, according to the MSM section, the freshwater layer in the fresher part of the front likely extended past the drogue depth centered at 15-m, so the drifter current represents a mix of the velocity in the freshwater surface layer and below it.

These different velocity estimates are in the same bulk range, and although the width of the associated velocity structure is not the same between MSM and Atalante surface data, these larger velocities in the 25–50 cm/s range close or just south of the front (near the freshwater bulge) are close to the expected velocity of an internal gravity current assuming a Froude number of 1 (with the change in stratification of a little over 1 pss and layer thickness of ~ 20 m). The velocity data suggest a front/gravity current propagating to the northwest or west with respect to the underlying water at the time it was crossed. Such a propagating front would quickly spread (by 20–40 km/day) the freshest shelf surface waters on top of the less fresh waters found on the other side of the front, contributing to increased stratification of salinity and density. Further investigation is required to better understand what sets this front and its characteristics, and how it sheds internal waves, as is known to happen in freshwater plumes of riverine origin (Nash & Moum, 2005).

4.3. Thickness of the Freshwater Layer

The freshwater layers appeared to have a shallow MLD even at night on February 5th, with a stratified layer reaching to within 10 m of the surface. This stratification is also observed on the earlier sections on February 2nd, and in the drifter data during the first 5 days after deployment and as the fresh water starts separating from the shelf. However, the freshwater layer is thicker by 10–15 m or more in the MVP surveys just southwest of the surface front. These different sections were positioned rather close to the north-western edge of the fresh water penetrating from the shelf, based on the daily SSS maps. This is also the case for the drifters, with the salinity map in Figure 6 for the last day of the trajectories on February 7th suggesting close proximity of the drifters to the front. MLD is somewhat deeper by February 17th–18th from the indirect estimate of the Saildrone (at least 17 m), though potentially with a large uncertainty as density profiles were not measured. Nevertheless, the difference between the two estimates suggests that there has been some vertical mixing and entrainment of deeper saltier water into the shallow surface fresh water during these 14 days. Thus, this is coherent with the velocity profiles suggesting active turbulence in the fresh plume stratified salinity layer.

Such shallow layers also imply that the drogue of the SVP drifters, which is between 12-m and 20-m depth, is only partially within the surface mixed layer, at least at their deployment in the initial freshwater plume. Their drift might thus differ from the speed of the freshest surface water, possibly explaining why most drifters deployed in the freshwater plume ultimately crossed the salinity fronts to the west of the freshwater plume (near these fronts, Ekman transport tended to be to the right of the drifter trajectories). The observations from Ocarina on the shelf in a salinity stratified layer (although much less stratified than in areas of lowest surface salinity), also indicated strong shear of the current within the top 17 m (close to 40 cm/s shear between depths of 1 and 17 m). Such shear and shallow layer imply a strong slippage of the surface layer relative to the layer just below, which could explain the fast spreading to the north and north-west of the freshwater plume.

5. Conclusions

In early February 2020, in the core of the saltiest and driest period, a freshwater plume was observed by satellite and in situ data entering the deep north-western tropical Atlantic near 54°W. This changes the perception that during this period, freshwater transport would take place mainly on the shelf and close to the shelf break. This plume was initially very surface trapped with stratification up to 10-m depth and with a width on the order of 120 km. Its freshwater content corresponded to 2–3 m of Amazon water and was distributed down to 40 m, although most of its water was found in the top 20 m. The off-shelf transport lasted for at least 10 days with freshwater transport comparable to the Amazon outflow in January. The plume was still quite well defined 16 days after it started spreading off the shelf break to reach a maximum area of 100,000 km², and up to 400 km further north. At this time, the mixed layer had not deepened to more than 20 m as indicated by current profiler data during a Saildrone transect. Although this is difficult to put into context from the limited in situ data, the mixed layer in the plume was shallower than night-time mixed layers found nearby in saltier waters.

A slight change in wind direction along the shelf between the Amazon estuary and 6°N for more than 3 days in late January seems to have triggered the north-westward flow of Amazon freshwater along the shelf and toward the shelf break. The low salinities might also have been sustained by fairly large Amazon outflow in late January compared to other years, estimated from the high river levels reported by altimetry on hydroweb.theia-land.fr. The off-shelf freshwater plume was steered by eddies, and in particular by a nearly stationary anti-cyclonic NBC ring up to 12°N. It also spread toward the Caribbean, due to the evolution of the different mesoscale eddies and to the Ekman transport. This fits with the freshwater pathway (a) in Coles et al. (2013) that they suggest is common from February to May.

The presence of such events of freshwater transport in February is documented since 2010 in 7 out of 10 years, where changes in wind direction closer to the equator concomitant to the presence of anticyclonic eddies to the east of the plume separation from the shelf seems to have contributed to their development and evolution. Such events should contribute largely to a freshening of the surface salinity in February/March north of the Guiana shelves and south of 12°N. It seems that the mechanism at work here is rather

different than what was commented for anomalies later in the year leading to boreal summer, where both current anomalies and wind anomalies, as well as the interannual anomalies of Amazon outflow, or conditions upstream (south of the equator) seem to play important roles.

The position of the 2020 plume's first offshore extension near 54°W is eastward compared to the other plumes detected in CCI products for the other years (Figure S3). We found that such freshwater plumes in February are not rare, and are also commonly associated with the NBC rings such as A1 that was nearly stationary during the plume development and retract water from shelf region into the open ocean. The stationarity is likely linked to the bathymetry of the Demerara Rise to its west that might act to trap/slow down eddies. Clearly more research on the frequency of this phenomenon and how it is modulated seasonally and interannually will be interesting. Inspecting CCI weekly salinity maps suggested that this process also seems to happen in March, and maybe early April, though this will require further investigation. Afterward in the spring season, with the seasonal wind changes and an increase in Amazon outflow, it is however likely that other processes involved in the development of interannual salinity anomalies in this region east of the lesser Antilles and north of the Guiana shelves might dominate, as suggested by Coles et al. (2013).

Data Availability Statement

We benefited from numerous data sets made freely available and listed here: the SLA and currents produced by Ssalto/Duacs distributed by the CMEMS (<https://resources.marine.copernicus.eu>), the Chl_a maps produced by CLS (also provided at <https://observations.ipsl.fr/aeris/eurec4a/#/>), the SMOS maps produced by CATDS (CATDS, 2019) (<https://10.12770/12dba510-cd71-4d4f-9fc1-9cc027d128b0>), and the SMAP maps produced by Remote Sensing System (also at <https://observations.ipsl.fr/aeris/eurec4a/#/>), as well as CCI+SSS maps produced in the frame of ESA CCI+SSS project (<https://10.5285/4ce685bff631459fb2a-30faa699f3fc5>). Among in situ data, Ocarina data are at <https://www.seanoe.org/data/00663/77479/>. All saildrone and salinity drifter data are available here: <https://psl.noaa.gov/thredds/catalog/Datasets/ATOM-IC/catalog.html>, and other oceanographic data collected on the research vessels (TSG, uCTD, MVP profiles) are on site <https://observations.ipsl.fr/aeris/eurec4a/#/>

Acknowledgments

This work is a contribution to the LEFE/IMAGO-GMMC project EUREC⁴A-OA, to the JPI-Climate and JPI Oceans project EUREC⁴A-OA, and to the TOSCA SMOS-Ocean project supported by CNES (Centre National d'Etudes Spatiales). Support was also obtained from IFREMER, the French Research Fleet, the French Research Infrastructures AERIS and ODATIS, IPSL, the "Chaire Chanel" of the Geosciences Department at ENS and the European Union's Horizon 2020 research and innovation program under grant agreement no. 817578 TRIATLAS. L. Olivier was supported by a scholarship from ENS and Sorbonne Université. Support for the salinity drifters was provided by the Climate Variability and Predictability Program of NOAA's Climate Program Office. MSM observations benefit from MOSES observational infrastructure. G. R. Foltz was supported by base funds to NOAA/AOML's Physical Oceanography Division. D. Zhang was supported by NOAA's Climate Program Office, Climate Variability and Predictability Program, and the Joint Institute for the Study of the Atmosphere and Ocean (JISAO) under NOAA Cooperative Agreement NA15OAR4320063.

References

- Bourras, D., Cambra, R., Marié, L., Bouin, M. N., Baggio, L., Branger, H., et al. (2019). Air-sea turbulent fluxes from a wave-following platform during six experiments at sea. *Journal of Geophysical Research: Oceans*, 124, 4290–4321. <https://doi.org/10.1029/2018jc014803>
- Boutin, J., Vergely, J.-L., Marchand, S., d'Amico, F., Hasson, A., Kolodziejczyk, N., et al. (2018). New SMOS sea surface salinity with reduced systematic errors and improved variability. *Remote Sensing of Environment*, 214, 115–134. <https://doi.org/10.1016/j.rse.2018.05.022>
- Carrasco, R., Horstmann, J., & Seemann, J. (2017). Significant wave heights measured by Coherent X-band radar. *IEEE Transactions on Geoscience and Remote Sensing*, 55(9), 5355–5365. <https://doi.org/10.1109/TGRS.2017.2706067>
- CATDS. (2019). *CATDS-PDC L3OS 2Q – Debaised daily valid ocean salinity values product from SMOS satellite*. CATDS (CNES, IFREMER, LOCEAN, ACRI). <https://doi.org/10.12770/12dba510-cd71-4d4f-9fc1-9cc027d128b0>
- Coles, V. J., Brooks, M. T., Hopkins, J., Stukel, M. R., Yager, P. L., & Hood, R. R. (2013). The pathways and properties of the Amazon River plume in the tropical North Atlantic Ocean. *Journal of Geophysical Research: Oceans*, 118, 6894–6913. <https://doi.org/10.1002/2013JC008981>
- Dankert, H., & Horstmann, J. (2007). A marine radar wind sensor. *Journal of Atmospheric and Oceanic Technology*, 24(9), 1629–1642. <https://doi.org/10.1175/jtech2083.1>
- Dibarboure, G., Pujol, M.-I., Briol, F., Le Traon, P.-Y., Larnicol, G., Picot, N., et al. (2011). Jason-2 in DUACS: Updated system description, first tandem results and impact on processing and products. *Marine Geodesy*, 2(34), 214–241. <https://doi.org/10.1080/01490419.2011.584826>
- Entekhabi, D., Njoku, E. G., O'Neill, P. E., Kellogg, K. H., Crow, W. T., Edelstein, W. N., et al. (2010). The soil moisture active passive (SMAP) mission. *Proceedings of the IEEE*, 98(5), 704–716.
- Foltz, G. R., Hummels, R., Dengler, M., Perez, R. C., & Araujo, M. (2020). Vertical turbulent cooling of the mixed layer in the Atlantic ITCZ and trade wind regions. *Journal of Geophysical Research: Oceans*, 125, e2019JC015529. <https://doi.org/10.1029/2019JC015529>
- Foltz, G. R., Schmid, C., & Lumpkin, R. (2018). An enhanced PIRATA data set for tropical Atlantic Ocean-atmosphere research. *Journal of Climate*, 31, 1499–1524. <https://doi.org/10.1175/JCLI-D-16-0816.1>
- Font, J., Camps, A., Borges, A., Martin-Neira, M., Boutin, J., Reul, N., et al. (2009). SMOS: The challenging sea surface salinity measurement from space. *Proceedings of the IEEE*, 98(5), 649–665.
- Fournier, S., Chapron, B., Salisbury, J., Vandermark, D., & Reul, N. (2015). Comparison of spaceborne measurements of sea surface salinity and colored detrital matter in the Amazon plume. *Journal of Geophysical Research: Oceans*, 120, 3177–3192. <https://doi.org/10.1002/2014jc010109>
- Fournier, S., Vandermark, D., Gaultier, L., Lee, T., Jonsson, B., & Gierach, M. M. (2017). Interannual variation in offshore advection of Amazon-Orinoco plume water: Observations, forcing mechanisms, and impacts. *Journal of Geophysical Research: Oceans*, 122, 8966–8982. <https://doi.org/10.1002/2017jc013103>
- Fratantoni, D. M., & Glickson, D. A. (2002). North Brazil current ring generation and evolution observed with SeaWiFS. *Journal of Physical Oceanography*, 32, 1058–1074. [https://doi.org/10.1175/1520-0485\(2002\)032<1058:nbcrga>2.0.co;2](https://doi.org/10.1175/1520-0485(2002)032<1058:nbcrga>2.0.co;2)

- Galperin, B., Sukoriansky, S., & Anderson, P. S. (2007). On the critical Richardson number in stably stratified turbulence. *Atmospheric Science Letters*, 8, 65–69. <https://doi.org/10.1002/asl.153>
- Geyer, W. R., Beardsley, R. C., Candela, J., Castro, B. M., Legeckis, R. V., Lentz, S. J., et al. (1991). The physical oceanography of the Amazon outflow. *Oceanography*, 4(1), 8–14. <https://doi.org/10.5670/oceanog.1991.15>
- Grodsky, S. A., Reverdin, G., Carton, J. A., & Coles, V. J. (2014). Year-to-year salinity changes in the Amazon plume: Contrasting 2011 and 2012 Aquarius/SACD and SMOS satellite data. *Remote Sensing of Environment*, 140, 14–22. <https://doi.org/10.1016/j.rse.2013.08.033>
- Grodsky, S. A., Vandermark, D., & Feng, H. (2018). Assessing coastal SMAP surface salinity accuracy and its application to monitoring Gulf of Maine circulation dynamics. *Remote Sensing*, 10(8), 1232. <https://doi.org/10.3390/rs10081232>
- Hu, C., Montgomery, E. T., Schmitt, R. W., & Muller-Karger, F. E. (2004). The dispersal of the Amazon and Orinoco River water in the tropical Atlantic and Caribbean Sea: Observation from space and S. PALACE floats. *Deep Sea Research Part II*, 51, 1151–1171. [https://doi.org/10.1016/s0967-0645\(04\)00105-5](https://doi.org/10.1016/s0967-0645(04)00105-5)
- Huang, W., Carrasco, R., Shen, C., Gill, E. W., & Horstmann, J. (2016). Surface current measurements using X-band marine radar with vertical polarization. *IEEE Transactions on Geoscience and Remote Sensing*, 54(5), 2988–2997. <https://doi.org/10.1109/tgrs.2015.2509781>
- Johns, W. E., Zantopp, R. J., & Goni, G. J. (2003). Cross-gyre transport by North Brazil Current rings. In G. J. Goni, & P. Malanotte-Rizzoli (Eds.), *Interhemispheric water exchange in the Atlantic Ocean* (pp. 411–441), Elsevier.
- Kerr, Y. H., Waldteufel, P., Wigneron, J.-P., Delwart, S., Cabot, F., Boutin, J., et al. (2010). The SMOS mission: New tool for monitoring key elements of the global water cycle. *Proceedings of the IEEE*, 98(5), 666–687. <https://doi.org/10.1109/jproc.2010.2043032>
- Laxenaire, R., Speich, S., Blanke, B., Chaigneau, A., & Pegliasco, C. (2018). Anticyclonic eddies connecting the western boundaries of Indian and Atlantic oceans. *Journal of Geophysical Research: Oceans*, 123(11), 7651–7677. <https://doi.org/10.1029/2018JC014270>
- Lentz, S. J. (1995). The Amazon river plume during AMASSEDs: Subtidal current variability and the importance of wind forcing. *Journal of Geophysical Research*, 100, 2377–2390. <https://doi.org/10.1029/94jc00343>
- Lund, B., Haus, B. K., Horstmann, J., Graber, H. C., Carrasco, R., Laxague, J. M., et al. (2018). Near-surface current mapping by ship-board marine X-band radar: A validation. *Journal of Atmospheric and Oceanic Technology*, 35(5), 1077–1090. <https://doi.org/10.1175/jtech-d-17-0154.1>
- Mignot, J., Lazar, A., & Lacarra, M. (2012). On the formation of barrier layers and associated vertical temperature inversions: A focus on the northwestern tropical Atlantic. *Journal of Geophysical Research*, 117, C02010. <https://doi.org/10.1029/2011JC007435>
- Muller-Karger, F. E., Mc Lain, C. R., & Richardson, P. L. (1988). The dispersal of the Amazon's water. *Nature*, 333, 56–58. <https://doi.org/10.1038/333056a0>
- Nash, J. D., & Moum, J. M. (2005). River plumes as a source of large-amplitude internal waves in the coastal ocean. *Nature*, 437, 400–403. <https://doi.org/10.1038/nature03936>
- Piepmeyer, J. R., Focardi, P., Horgan, K. A., Knuble, J., Ehsan, N., Lucey, J., et al. (2017). SMAP L-band microwave radiometer: Instrument design and first year on orbit. *IEEE Transactions on Geoscience and Remote Sensing*, 55(4), 1954–1966. <https://doi.org/10.1109/tgrs.2016.2631978>
- Reul, N., Grodsky, S. A., Arias, M., Boutin, J., Catany, R., Chapron, B., et al. (2020). Sea surface salinity estimates from spaceborne L-band radiometers: An overview of the first decade of observation (2010–2019). *Remote Sensing of Environment*, 242, 111769. <https://doi.org/10.1016/j.rse.2020.111769>
- Rio, M. H., Guinehut, S., & Larnicol, G. (2011). New CNES CLS09 global mean dynamic topography computed from the combination of GRACE data, altimetry, and in-situ measurements. *Journal of Geophysical Research*, 116, C07018. <https://doi.org/10.1029/2010jc006505>
- Salisbury, J., Vandemark, D., Campbell, J., Hunt, C., Wisser, D., & Reul, N. (2011). Spatial and temporal coherence between Amazon River discharge, salinity, and light absorption by colored organic carbon in western tropical Atlantic surface waters. *Journal of Geophysical Research*, 116, C00H02. <https://doi.org/10.1029/2011JC006989>
- Senet, C. M., Seemann, J., & Ziemer, F. (2001). The near-surface current velocity determined from image sequences of the sea surface. *IEEE Transactions on Geoscience and Remote Sensing*, 39(3), 492–505. <https://doi.org/10.1109/36.911108>
- Steinmetz, F., Deschamps, P. Y., & Ramon, D. (2011). Atmospheric correction in presence of sun glint: Application to MERIS. *Optics Express*, 19(10), 9783–9800. <https://doi.org/10.1364/oe.19.009783>
- Stevens, B., Sandrine, B., David, F., Felix, A., Alan, B., Christopher, F., et al. (2021). EUREC4A. Submitted to Earth System science data. Retrieved from <https://essd.copernicus.org/preprints/essd-2021-18/>
- Stum, J., Tebri, H., Lehodey, P., Senina, I., Greiner, E., Lucas, M., & Steinmetz, F. (2015). NRT operational chlorophyll maps for marine applications. Poster presented at the 2nd IOCS meeting, San Francisco, CA. Retrieved from <http://www.eposters.net/pdfs/nrt-operational-chlorophyll-maps-calculation-for-marine-applications.pdf>
- Taburet, G., Sanchez-Roman, A., Ballarotta, M., Pujol, M. I., Legeais, J.-F., Fournier, F., et al. (2019). DUACS DT2018: 25 years of reprocessed sea level altimetry products. *Ocean Science*, 15, 1207–1224. <https://doi.org/10.5194/os-15-1207-2019>
- Zhang, D., Cronin, M. F., Meinig, C., Farrar, J. T., Jenkins, R., Peacock, D., et al. (2019). Comparing Air-sea flux measurements from a new unmanned surface vehicle and proven platforms during the SPURS-2 field campaign. *Oceanography*, 32(2), 122–133. <https://doi.org/10.5670/oceanog.2019.220>